Pergamon

Int. J. Multiphase Flow Vol. 24, No. 2, pp. 271–281, 1998

Printed in Great Britain
PII: S0301-9322(97)00047-5
0301-9322/98 $19.00 + 0.00

A NUMERICAL MODEL OF TAYLOR BUBBLES RISING THROUGH STAGNANT LIQUIDS IN VERTICAL TUBES

J. D. BUGG, K. MACK and K. S. REZKALLAH
Department of Mechanical Engineering, The University of Saskatchewan, 57 Campus Drive, Saskatoon, Saskatchewan S7N 5A9, Canada

(Received 20 December 1996; in revised form 16 June 1997)

Abstract—The motion of large bubbles in tubes is investigated numerically with a two-dimensional, transient, finite difference model using a volume fraction specification to track the movement of the gas–liquid interface. The terminal speed of the bubbles is well predicted for $10 \leq Eo \leq 100$ and $10^{-12} \leq Mo \leq 10^{1}$. The ubiquitous prolate spheroid leading edge is predicted. Both viscosity-dominated equilibrium films and essentially inviscid accelerating films are observed on the tube wall. The shape of the trailing edge is flat in some cases and an oblate spheroid in other cases. A criterion of $Fr > 0.3$ seems to be appropriate to ensure a flat bottom on the bubble. Some favourable comparisons are made with detailed velocity profile measurements available in the literature. © 1998 Elsevier Science Ltd. All rights reserved

Key Words: Taylor bubbles, free boundaries, interface advection, slug flow

1. INTRODUCTION

Gas bubbles moving through liquids in tubes occur widely in hydrocarbon production and transportation, chemical and nuclear reactors, and heat transport systems where phase change takes place. The distribution of the gas in the tube greatly influences the hydrodynamics, heat transfer, and mass transfer. One of the flow regimes commonly observed is slug flow where large, elongated bubbles are separated by slugs of liquids that usually contain small gas bubbles. In general, a variety of possible fluid properties, tube orientations, and liquid and gas flow rates produce these bubbles. A simplified configuration of considerable fundamental interest is the case of a vertical tube and zero liquid flow. This paper describes numerical predictions of the detailed bubble shape, velocity field, and pressure field for this case over a wide range of conditions.

The experimental results of White and Beardmore (1962) provide an excellent summary of Taylor bubble terminal speeds. They identify the Froude number ($U_t/\sqrt{gD}$), Eötvös number ($\rho g D^2/\sigma$), and Morton number ($g\eta^4/(\rho\sigma^3)$) as the important dimensionless groups. In these groups U_t is the terminal speed, g is the acceleration due to gravity, D is the tube diameter, ρ is the liquid density, σ is the surface tension, and η is the dynamic viscosity of the liquid. Other workers have also used the Reynolds number and the Weber number as parameters. Experiments have been carried out for a wide range of tube diameters and liquid properties. By including the data of several other workers, they produced a comprehensive graphical correlation of Froude number as a function of Eötvös number and Morton number. The correlation covers the range $3 < Eo < 400$ and $10^{-12} < Mo < 10^{3}$. They concluded that viscous forces are negligible if $\rho^2 g D^3/\eta^2 > 3 \times 10^5$, interfacial effects are negligible if $Eo > 70$, and inertial effects are negligible if $Fr < 0.05$.

Fabre and Liné (1992) reviewed the motion of Taylor bubbles as part of a larger review of slug flow. They specifically considered the case of zero liquid flow in vertical tubes. They stated that Taylor bubbles were characterised by leading edges shaped like prolate spheroids followed by a film on the wall of the tube and finally a trailing edge. This trailing edge would be flat in cases were viscosity is unimportant and would be an oblate spheroid in cases where viscosity is important. The groups they used to characterise slug flow are the Eötvös number and a 'dimensionless inverse viscosity', $N_f = (Eo^3/Mo)^{1/4} = \sqrt{\rho^2 g D^3/\eta^2}$. When viscous forces and surface ten-

sion forces are negligible ($N_f > 300$ and $Eo > 100$) the Froude number is 0.351. Surface tension tends to reduce this Froude number and they cite a result due to Bendiksen (1985) which adjusts Froude for $Eo < 100$. They state that the viscous regime is encountered for $N_f < 2$ and in this regime $Fr = 0.1N_f$. However, for intermediate values of N_f, no predictive method for Fr is given.

DeJesus *et al.* (1995) made detailed velocity field measurements around a Taylor bubble rising in a vertical tube using photochromic dye activation and image analysis. Velocity vectors were presented for the region near the bubble nose, in the falling film, and in the wake. The conditions reported correspond to $Eo = 194$ and $Mo = 2.9 \times 10^{-9}$.

Mao and Dukler (1990, 1991) developed a numerical model of the flow around a Taylor bubble using a curvilinear coordinate system attached to the bubble and fitted to the bubble shape. The technique adjusted the shape of the interface so that the normal stress at the interface satisfied the condition of constant pressure inside the bubble. The terminal velocity of the bubble, and therefore the reference frame velocity, was adjusted until the bubble was locally spherical at the nose. The solution domain extended only to the trailing edge of the bubble and not into the wake region.

Although numerical predictions of Taylor bubble movement do exist in the literature (Mao and Dukler 1991) this paper covers a wider range of conditions than have been reported to date. Also, the present work makes no *a priori* assumption about the shape of the leading edge or the terminal speed. The solution domain in the present model extends behind the bubble, allowing field information to be obtained in the wake region.

A technique very similar to that presented in this paper has been applied by Bugg and Rowe (1991) to the case of large cylindrical and spherical bubbles released from rest into infinite quiescent fluids. This work concentrated on the large deformation that occurs as the bubble transforms to cylindrical and spherical cap shapes. Although this transformation process was predicted very well, the subsequent steady motion of the caps proved challenging because of interface advection difficulties caused by the cusped edge of the bubble.

2. NUMERICAL MODEL

2.1. *Governing equations and discretisation*

In the liquid phase, the model considers the Navier–Stokes equations and the continuity equation in a cylindrical coordinate system for an incompressible fluid.

$$\frac{\partial v_r}{\partial t} + v_r \frac{\partial v_r}{\partial r} + v_z \frac{\partial v_r}{\partial z} = -\frac{1}{\rho}\frac{\partial P}{\partial r} + \frac{\eta}{\rho}\left(\frac{\partial^2 v_r}{\partial r^2} + \frac{1}{r}\frac{\partial v_r}{\partial r} + \frac{\partial^2 v_r}{\partial z^2} - \frac{v_r}{r^2}\right), \quad [1]$$

$$\frac{\partial v_z}{\partial t} + v_r \frac{\partial v_z}{\partial r} + v_z \frac{\partial v_z}{\partial z} = -\frac{1}{\rho}\frac{\partial P}{\partial z} + \frac{\eta}{\rho}\left(\frac{\partial^2 v_z}{\partial r^2} + \frac{1}{r}\frac{\partial v_z}{\partial r} + \frac{\partial^2 v_z}{\partial z^2}\right) + g, \quad [2]$$

$$\frac{\partial v_r}{\partial r} + \frac{\partial v_z}{\partial z} + \frac{v_r}{r} = 0. \quad [3]$$

In these equations, v_r and v_z are the radial and axial components of velocity, respectively, t is time, r and z are the radial and axial coordinates, and P is the pressure. These equations are discretised by finite differences on a uniform ($\delta r = \delta z$) staggered grid. By expressing the local acceleration in the Navier–Stokes equations by a first-order, forward-difference in time, an explicit approximation to the velocity field $\tilde{\mathbf{V}}$ is calculated. For example, the axial direction would appear as:

$$\frac{\tilde{v}_z - v_z^n}{\delta t} = -((\mathbf{V} \cdot \nabla)v_z)^n - \frac{1}{\rho}\left(\frac{\partial P}{\partial z}\right)^n + \nu(\nabla^2 v_z)^n, \quad [4]$$

where $\tilde{v}_z$ represents the axial component of the approximate velocity field $\tilde{\mathbf{V}}$ and the n superscripts indicate explicit evaluation of the convective and viscous terms. The convective accelera-

tion is hybrid differenced and the viscous stress is central differenced. The divergence ($\nabla \cdot \tilde{\mathbf{V}}$) in this velocity field is driven to zero by a pressure correction procedure formulated from the discretised continuity equation. The velocity corrections required to correct for zero divergence are related to the pressure corrections by (for example):

$$\Delta v_z = -\frac{\delta t}{\rho}\left(\frac{\partial \Delta P}{\partial z}\right). \quad [5]$$

This yields the following pressure correction equation for liquid-filled control volumes:

$$\Delta P_{i,j} 2\left(\frac{\delta r}{\delta z}+\frac{\delta z}{\delta r}\right) - \Delta P_{i-1,j}\left(\frac{\delta z}{\delta r}-\frac{\delta z}{2r^2}\right) - \Delta P_{i+1,j}\left(\frac{\delta z}{\delta r}+\frac{\delta z}{2r^2}\right) - \Delta P_{i,j-1}\frac{\delta r}{\delta z} - \Delta P_{i,j+1}\frac{\delta r}{\delta z} = -\frac{\rho \delta r \delta z}{\delta t}(\nabla \cdot \tilde{\mathbf{V}})_{i,j}. \quad (6)$$

Here the indices i,j denote position in the discrete grid and the pressure correction ΔP updates the P field according to $P^{n+1} = P^n + \Delta P$ where the superscript n refers to the time step.

The position of the moving gas–liquid interface in the solution domain is defined by a fractional volume of fluid f as suggested by Hirt and Nichols (1981). Liquid-filled control volumes ($f = 1$) use the pressure correction procedure just described. The Navier–Stokes equations are not solved for gas-filled control volumes ($f = 0$). They have $\Delta P = 0$ applied for the purpose of the linear system in ΔP. For control volumes containing a gas–liquid interface ($0 < f < 1$), [6] is replaced with one that imposes the normal interfacial boundary condition. The goal is to impose a pressure at the centre of the surface control volume such that a linear interpolation of pressure to the centre of the nearest liquid-filled neighbour will result in the proper pressure at the interface. The distance of the 'nearest liquid-filled neighbour' is determined by favouring interpolation perpendicular to the interface. The interpolation is accomplished by the following:

$$P_{ij}^{n+1} = \eta_{ij} P_s + (1-\eta_{ij}) P_{lm}^{n+1}, \quad [7]$$

which can be re-cast in terms of pressure corrections as:

$$\Delta P_{ij} + (\eta_{ij} - 1)\Delta P_{lm} = \eta_{ij} P_s + (1-\eta_{ij})\Delta P_{lm}^n - P_{ij}^n. \quad [8]$$

In this equation, ΔP_{ij} is the pressure correction in the surface control volume, ΔP_{lm} is the pressure correction in the nearest full control volume, the superscript n refers to quantities at the previous time step, and η_{ij} is an interpolation factor calculated from the position of the interface. P_s is the pressure on the liquid side of the interface and is calculated from the pressure in the gas and the effect of surface tension. Surface tension effects are included by calculating the local interface curvature from gradients in the f field. The tangential stress on the gas–liquid interface is zero in this work.

The system of linear equations [6] and [8] is solved for the pressure corrections ΔP. From these pressure corrections, velocity corrections can be obtained to update the velocity field from $\tilde{\mathbf{V}}$ to $\mathbf{V}^{n+1}$. The interface is now advected before the pressure correction procedure begins the next time step.

Formally, interface advection amounts to solving the pure advection equation

$$\frac{\partial f}{\partial t} + v_r \frac{\partial f}{\partial r} + v_z \frac{\partial f}{\partial z} = 0. \quad [9]$$

Standard differencing schemes applied to this equation suffer from diffusion which makes it difficult to maintain a distinct interface. Therefore, most techniques resort to a tracking scheme based on geometrical considerations and local interface reconstruction from the f field information. In this work the donor–acceptor algorithm of Hirt and Nichols (1981) is used to calculate the fluid fluxes across control volume faces. Gas regions less than the grid size are treated as being liquid-filled.

Since an explicit technique is used, the CFL condition must be satisfied when selecting a time step. The advection algorithm demands the same restriction on δt. The time step varied dramati-

cally over the run matrix, but 10^{-5} s was a typical value. A total simulation time of 0.5 to 1.0 s was used for these runs.

2.2. *Boundary conditions*

No slip boundary conditions were used on all solid boundaries. The domain represents a closed end tube so these conditions apply to the ends of the domain as well as the pipe wall. This boundary condition is imposed by setting the normal velocity to zero and specifying the tangential velocity at a virtual node outside the domain to a value which, when linearly interpolated to the first interior node, gives a velocity of zero at the wall.

2.3. *Model geometry*

A cylindrical coordinate system (r, z) assuming axial symmetry about the centreline of the pipe was used. All runs, except for the grid sensitivity study, were done with a 25×400 uniform grid. Therefore, for a pipe diameter of D, the length of the solution domain was $8D$. Although this paper focuses on the steadily rising Taylor bubble, the results were obtained with a transient model. The two initial conditions of the gas bubble are shown in figure 1. The gas volume in both cases was initially $\pi D^3/3$, twice the volume of a sphere of diameter D. This produced bubbles that were at least two tube diameters long. White and Beardmore (1962) indicate that the terminal speed is independent of the bubble length. Campos and Guedes de Carvalho (1988) studied wakes behind Taylor bubbles and established a criterion for minimum bubble length to make the wake flow independent of bubble length. Although most runs in the current research were for bubbles shorter than given by their criterion, no systematic study of the effect of length on wake structure was attempted as part of this work.

The liquid was initially quiescent. The initial pressure in the gas was equal to the hydrostatic pressure in the liquid at the depth of the bubble's centroid. The initial shape of the bubble affects only its temporal evolution and not the final shape attained. This was confirmed by testing several initial shapes other than those shown in figure 1.

2.4. *Gas pressure model*

The model calculates bubble volume from the volume fraction field, f. Changes in this volume result directly from changes in the f field calculated by the interface advection algorithm in response to the calculated velocity field. The gas pressure is adjusted at each time step based on an isentropic expansion/compression of the gas volume. An algorithm has been developed and implemented that recognises and accounts for any break-up or coalescence which occurs during

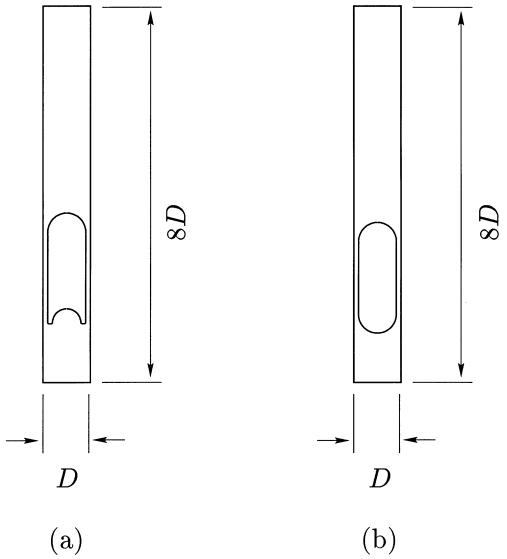

Figure 1. Initial gas configurations for Taylor bubble simulations: (a) cases one and two; (b) all other cases.

Table 1. Run conditions for steadily rising Taylor bubble simulations

	Case No.								
	1	2	3	4	5	6	7	8	9
log *Mo*	−12	−12	−12	−2	−2	−2	1	1	1
Eo	100	40	10	100	40	10	100	40	10
N_f	31,600	15,900	5,620	100	50	17.8	17.8	8.94	3.16

the simulation. In this case, the Taylor bubble was initially the only gas in the solution domain. Therefore, the volume and pressure of the bubble should be constant as it rises. In case one, small bubbles broke off as transition to the final shape occurred. Once there is more than one bubble in the solution domain, the constant pressure condition no longer applies since the volumes of the individual bubbles are no longer constant.

3. RESULTS AND DISCUSSION

The model was run for a variety of Eötvös and Morton numbers which are summarised in table 1. For this set of runs an assessment of bubble shape, terminal speed, and detailed velocity field information will be made.

Previous researchers have attempted to describe the bubble behaviour by identifying forces that may be either dominant or unimportant under particular conditions. These criteria, understandably, result in regimes were certain forces clearly dominate, separated by regions where several forces are important. According to the guidelines developed by White and Beardmore (1962), both surface tension and viscosity are negligible in case one. Cases two and three have negligible viscous forces ($N_f > 550$), while cases four and seven have negligible surface tension forces ($Eo > 70$). Cases six and nine have negligible inertia forces ($Fr < 0.05$). The other cases have no forces which can be considered negligible.

3.1. *Steady bubble shape*

Figure 2 summarises the final shapes predicted by the model for the full range of *Eo* and *Mo* investigated. The general features which will be discussed are the leading edge, the trailing edge, and the falling film. The classical Taylor bubble often observed in the laboratory usually results from air rising in water and has a prolate spheroidal leading edge and a flat, or even concave, trailing edge.

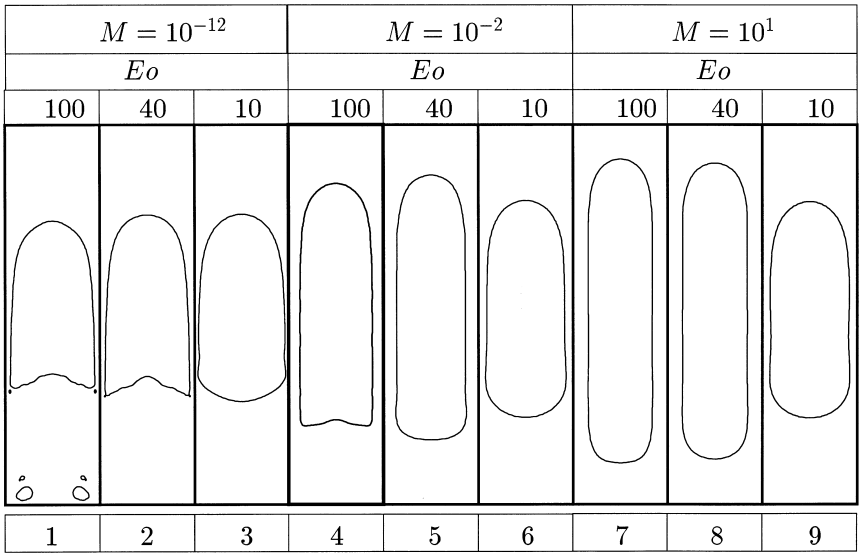

Figure 2. Steady Taylor bubble shapes for Eo = 100, 40, 10 and $M = 10^{-12}$, 10^{-2}, 10^{1} computed with a 25×400 grid.

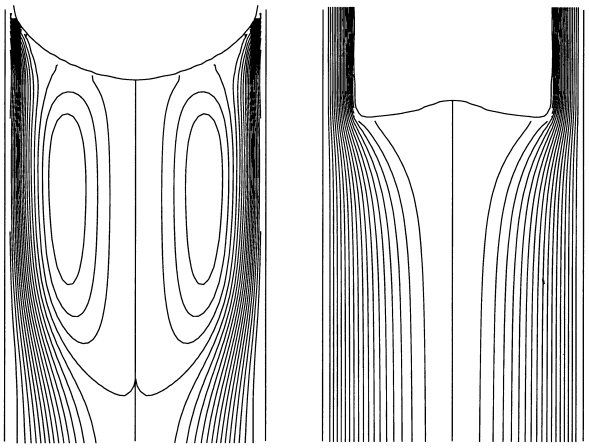

Figure 3. Streamlines immediately below bubbles for cases three and four.

3.1.1. *Leading edge*. The leading edge shape of the bubbles is their most universal feature. The shape is a prolate spheroid and occurs over the entire range of conditions modelled in this work. A quantitative comparison with experimental data will be made in Section 3.2.

3.1.2. *Trailing edge*. The results show flat or concave trailing edges for cases one, two, and four. Fabre and Liné (1992) state that the inertia-controlled regime is realised if $N_f > 300$ and that in this regime the bubbles have flat bottoms. White and Beardmore (1962) cite a criterion for negligible viscous effects equivalent to $N_f > 550$. In the current study, both N_f criteria are satisfied for cases one, two, and three. However, case three does not have a flat bottom even though it has an N_f of 5620. In addition, case four has a flat bottom even though N_f is only 100. A more detailed look at the flow immediately below these two bubbles may help (see figure 3). It is interesting that, although the bottom of case three is shaped like an oblate spheroid, there is a rather large recirculation region below the bubble. In contrast, case four has a flat bottom but displays no recirculation zone. Therefore, it appears that the streamlines are consistent with the expectation that a viscosity-dominated flow (case 4) would have no separation while an inertia-dominated flow would experience separation. However, under these conditions it appears that these flow characteristics do not translate into a spheroidal bottom for the viscous flow and a flat bottom for the inertial flow. A more clear criterion for a rounded bottom may be the Froude number. As can be seen in table 2, the three cases with flat bottoms all have a relatively high Froude number ($Fr > 0.3$).

3.1.3. *Falling film*. The film thickness will be discussed quantitatively in the next section, but some qualitative discussion will be given here. Cases one, two, and three show a film that continues to thin all the way to the trailing edge. These are the conditions for which White and Beardmore (1962) stated that viscous forces are unimportant, so the thinning film implies a freely falling film in these cases. All other runs have at least a portion of the film with constant thickness, indicating a falling film which has reached equilibrium.

Another general feature apparent in figure 2 is that the bubble lengths vary widely for the different runs. However, the volumes of all the bubbles are the same (except for case one where

Table 2. Predicted Froude number of steadily rising Taylor bubbles compared to the experimental data of White and Beardmore (1962)

	log *Mo* −12			log *Mo* −2			log *Mo* 1		
Eo	Model	Experimental	% Difference	Model	Experimental	% Difference	Model	Experimental	% Difference
100	0.346	0.34	1.8	0.323	0.30	7.7	0.170	0.15	13.
40	0.350	0.32	9.5	0.246	0.22	12	0.0713	0.065	8.0
10	0.179	0.17	5.0	0.0252	0.030	−16	0.00440	0.0048	−8.3

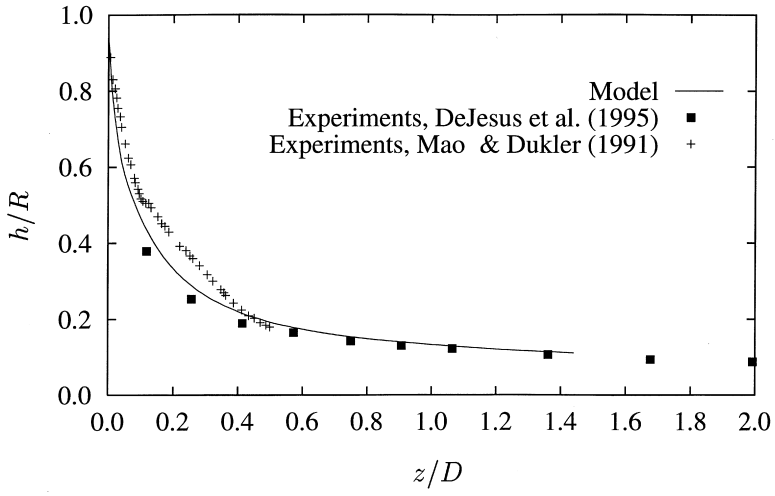

Figure 4. Film thickness for $Eo = 100$, $Mo = 10^{-12}$ compared to experimental data.

some small bubbles have been shed in the wake). The widely differing bubble lengths are attributable to different film thicknesses.

The small bubbles in the wake of case 1 in figure 2 must be interpreted correctly in light of the assumption of axial symmetry inherent in this two-dimensional model. Although they appear as small bubbles they are, of course, toroids once they are revolved around the axis of symmetry. The bubbles typically trapped between two Taylor bubbles in a slug flow are not toroidal but roughly spherical. These, of course, cannot be modelled in two dimensions. Therefore, the current model cannot provide insight into the complex interactions of small bubbles trapped in the recirculating wake.

3.2. *Film thickness*

The most common quantitative measure of Taylor bubble shape is the variation of film thickness with distance from the top of the bubble. Figure 4 show the current prediction for $Eo = 100$ and $Mo = 10^{-12}$ along with two experimental results. The first set of data is taken from DeJesus *et al.* (1995). Their conditions were $Eo = 194$ and $Mo = 2.9 \times 10^{-9}$. Although they did not directly report measurements of film thickness, they did report average film velocity vs axial position. They also report film thickness at a specific location and its corresponding average film velocity. By continuity considerations, the film thickness vs axial position can be inferred from these data. The second set of data is taken from Mao and Dukler (1991). Their conditions were $Eo = 337$ and $Mo = 2.5 \times 10^{-11}$ and measurements were only reported quite near the top of the bubble. The numerical results fall well within the experimental data.

3.3. *Terminal speed*

The variety of runs presented provides the opportunity to evaluate the terminal speed prediction of Taylor bubbles over a wide range of conditions. The run matrix includes regions where inertia, viscosity, and surface tension are each unimportant. A summary of the terminal speed predictions is given in table 2. The experimental results cited are taken from the general graphical correlation of White and Beardmore (1962). For most of the cases, the model overpredicts the terminal speed but is largely within 10% of the experimental data. The only cases where the terminal speed is underpredicted are cases six and nine, where White and Beardmore (1962) stated inertial effects were negligible. The predicted bubble shapes for these two cases are almost identical.

3.4. *Velocity field*

A detailed representation of the predicted velocity field for case one is shown in figure 5. This figure shows velocity vectors, streamlines, and velocity profiles at various axial locations. The velocity field shows the characteristics expected. Since this is an inertia-dominated flow, the

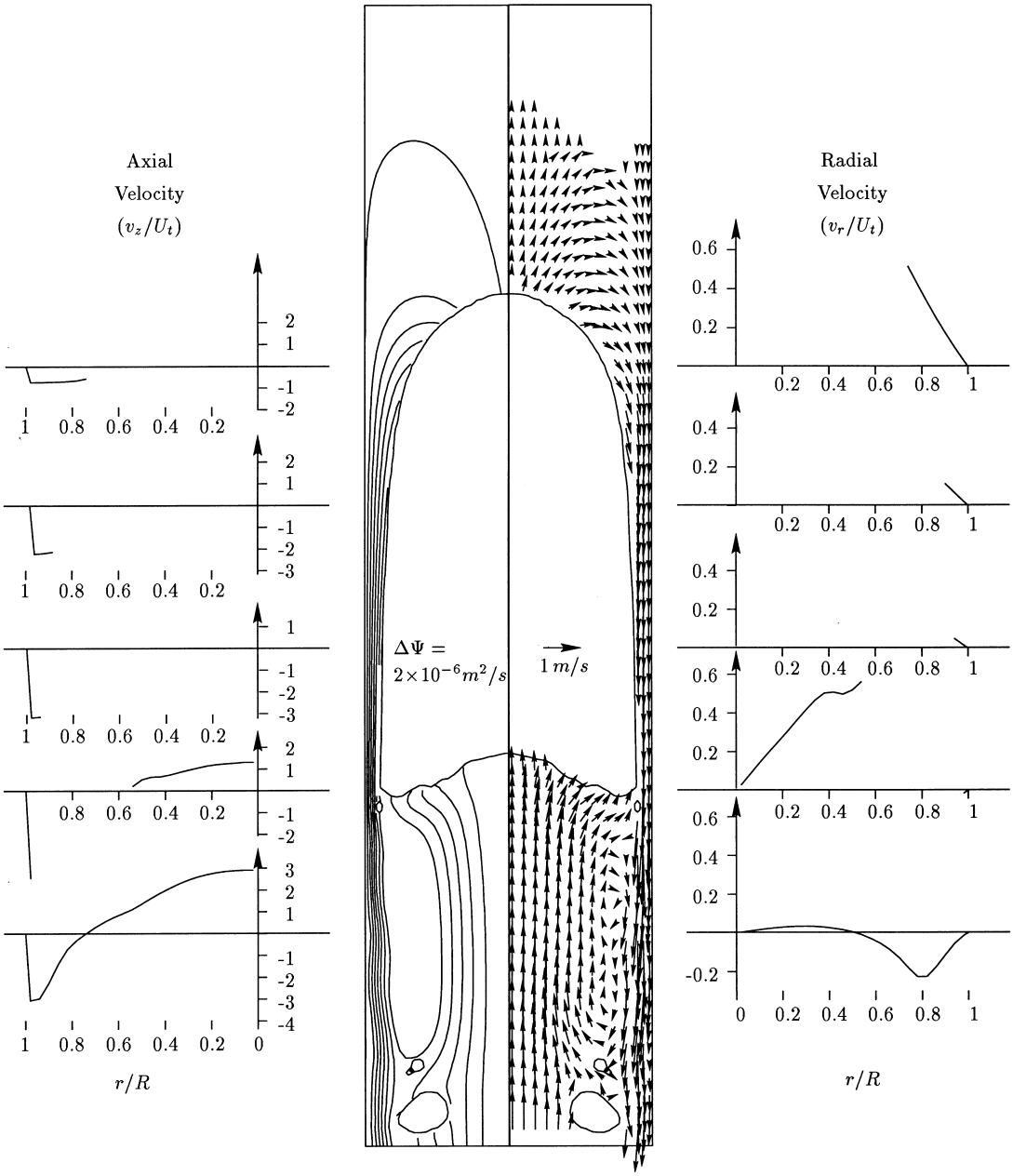

Figure 5. Detailed velocity field information for $Eo = 100$, $Mo = 10^{-12}$. The plots at the extreme left and right give the axial and radial velocity components normalised by the terminal velocity of the bubble. The left half of the centre plot shows lines of constant stream function while the right half shows velocity vectors.

axial velocity in the film is not a function of radial position. However, it does increase with axial position, resulting in a continually thinning film all the way to the trailing edge. A recirculation zone is apparent in the wake of the bubble which is driven by the relatively high velocity wall jet penetrating into the region below the bubble.

Figure 6 compares the axial velocity profiles in the film for case one and case seven. Both profiles are shown at a position $3D/4$ from the leading edge of the bubble. Velocities are normalised to the terminal velocity and distances from the wall, y, are normalised with the local film thickness. For case one, the viscosity is relatively unimportant and the velocity profile in the film is quite flat. Note, in fact, that the numerical model is not resolving the details of the boundary layer at all in this case. However, the prediction agrees very well with experiments because this boundary layer is relatively unimportant in determining the bubble shape and terminal velocity.

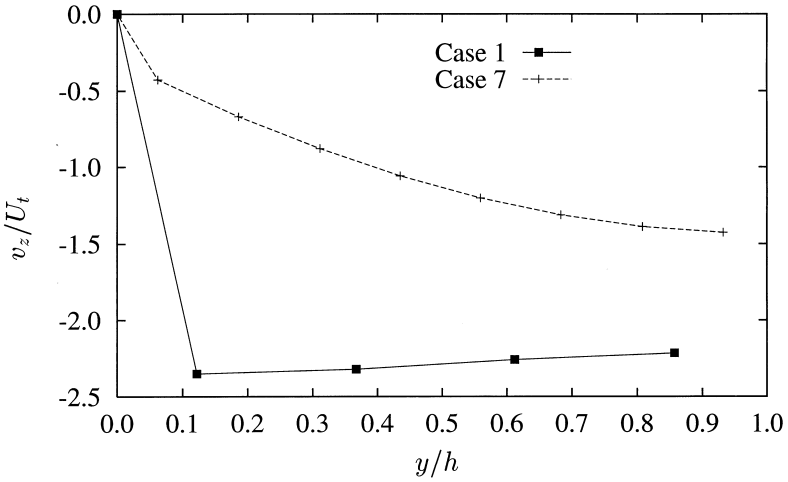

Figure 6. Comparison of film velocity profiles in cases one and seven.

In case seven, however, viscosity dominates and the boundary layer is much thicker. Therefore, the boundary layer can be adequately resolved and a reasonable prediction is again achieved. Because the wall shear force now equals the weight of the fluid in the film, the film is in equilibrium and therefore has constant thickness.

The experimental work of DeJesus *et al.* (1995) provides detailed velocity measurements around a rising Taylor bubble. Their work was done with air rising in kerosene within a 25.4 mm diameter tube yielding $Eo = 194$ and $Mo = 2.9 \times 10^{-9}$. According to the work of White and Beardmore (1962), these bubbles should behave the same as those with $Eo = 100$ and $M = 10^{-12}$. Both are in the regime were surface tension forces and viscosity are negligible. DeJesus *et al.* (1995) report velocity vectors at several axial planes along the length of the steadily rising bubble. They also report radially averaged film velocity at various axial locations. Figure 7 shows some of these data compared to the present predictions.

3.5. *Grid independence*

Confidence of grid independent results is gained from selected runs that were done with a 50×800 rather than a 25×400 grid. The results are very similar. A representative result is given in figure 8, which shows the shape of the bubble for both grids. In addition to this, the terminal speed for this case changed by less than 1% upon grid refinement.

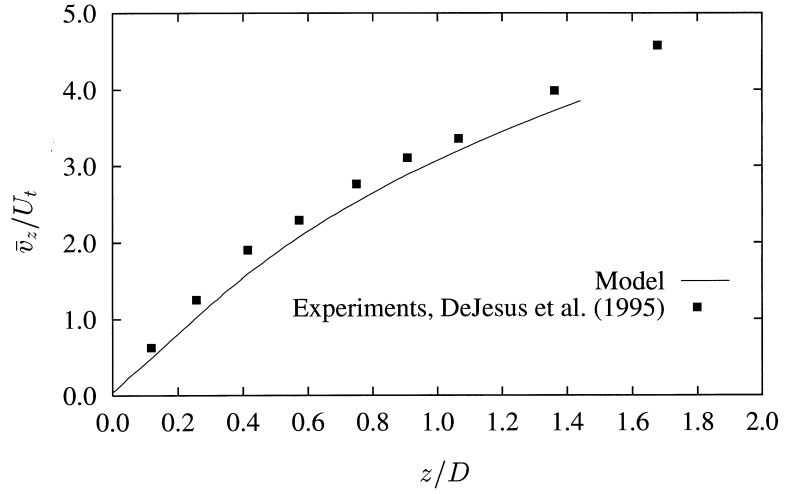

Figure 7. Average film velocity for $Eo = 100$, $Mo = 10^{-12}$ compared to experimental data.

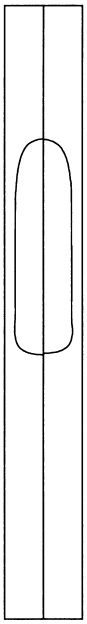

Figure 8. Grid independence test for $Eo = 40$, $M = 10^{-2}$. Left side of axis of symmetry calculated with a 50×800 grid; right side with a 25×400 grid.

4. CONCLUSIONS

It has been demonstrated that it is possible to numerically model several important features of steadily rising Taylor bubbles over a large range of conditions ($10 \leq Eo \leq 100$ and $10^{-12} \leq Mo \leq 10^{1}$). The terminal speed of the bubbles was well predicted. The film thickness and the average velocity in the film compared favourably with experimental data. From the results, several observations about Taylor bubble behaviour can be made.

1. The rounded leading edge exists for all conditions tested.
2. An equilibrium film thickness was achieved for all runs with $N_f \leq 100$.
3. A flat bottom was observed for all runs with $Fr > 0.3$.
4. Under certain conditions, a recirculation zone can occur below a rounded trailing edge. Also, a flat trailing edge can apparently exist with very little recirculation.

Acknowledgements—This work has been supported by the Canadian Natural Sciences and Engineering Research Council.

REFERENCES

Bendiksen, K. H. (1985) On the motion of long bubbles in vertical tubes. *Int. J. Multiphase Flow* **11,** 797–812.

Bugg, J. D. and Rowe, R. D. (1991) Modelling the initial motion of large cylindrical and spherical bubbles. *Int. J. Numerical Methods in Fluids* **13,** 109–129.

Campos, J. B. L. M. and Guedes de Carvalho, J. R. F. (1988) An experimental study of the wake of gas slugs rising in liquids. *J. Fluid Mechanics* **196,** 27–37.

DeJesus, J. D., Ahmad, W. and Kawaji, M. (1995) Experimental study of flow structure in vertical slug flow. In *Proc. 2nd Int. Conf. on Multiphase Flow*, Kyoto, 3–7 April.

Fabre, J. and Liné, A. (1992) Modelling of two-phase slug flow. *Ann. Rev. Fluid Mech.*, **24,** 21–46.

Hirt, C. W. and Nichols, B. D. (1981) Volume of fluid (VOF) method for the dynamics of free boundaries. *J. Comp. Phys.* **39,** 201–225.

Mao, Z.-S. and Dukler, A. E. (1990) The motion of Taylor bubbles in vertical tubes I. A numerical simulation for the shape and rise velocity of Taylor bubbles in stagnant and flowing liquids. *J. Comp. Phys.* **91,** 132–160.

Mao, Z.-S. and Dukler, A. E. (1991) The motion of Taylor bubbles in vertical tubes II. Experimental data and simulations for laminar and turbulent flow. *Chem. Eng. Sci.* **46,** 2055–2064.

White, E. T. and Beardmore, R. H. (1962) The velocity of rise of single cylindrical air bubbles through liquids contained in vertical tubes. *Chem. Eng. Sci.* **17,** 351–361.